

Distinct Speciation of Naphthalene Vapor Deposited on Ice Surfaces at 253 or 77 K: Formation of Submicrometer-Sized Crystals or an Amorphous Layer

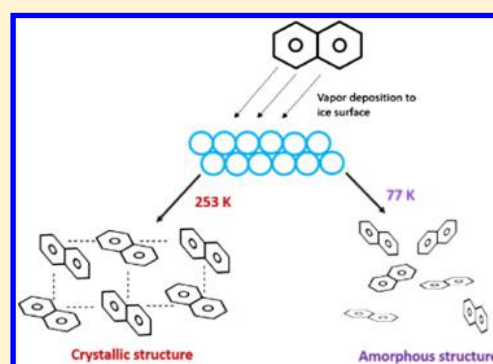
Gabriela Ondrušková,[†] Ján Krausko,[†] Josef N. Stern,[‡] Astrid Hauptmann,[‡] Thomas Loerting,[‡] and Dominik Heger^{*,†}

[†]Department of Chemistry and RECETOX, Faculty of Science, Masaryk University, Kamenice 5, 625 00 Brno, Czech Republic

[‡]Institute of Physical Chemistry, University of Innsbruck, Innrain 52c, A-6020 Innsbruck, Austria

Supporting Information

ABSTRACT: Naphthalene was deposited from the vapor phase on ice surfaces at 77 or 253 K to yield strongly distinct behavior, forming either an amorphous glass layer or submicrometer-sized crystals, respectively. The results stand upon optical emission spectroscopy combined with differential scanning calorimetry and X-ray analysis. The amorphous layer of naphthalene on the ice behaves in the same manner as on an inert metallic support: it starts to relax at 105 K and crystallizes at 185 K. The formed microcrystals exhibit distinct absorption behavior on the ice surface and are thus expected to have a photokinetic profile varying from freeze-concentrated solutions. The observations bring implications toward environmental and extraterrestrial ice sciences.



INTRODUCTION

The physical and chemical processes taking place at the air–ice interface have been studied extensively over the past decades.^{1,2} Frozen water, regardless of whether it assumes the form of a snowpack or icebergs, airborne ice crystals, aerosols, or interstellar and cometary ice,³ plays an important role in the chemistry of volatile compounds present in these particular environments. Our gradually growing understanding of compounds' speciation on/in ice is still rather limited, especially as the location of impurities is determined not only by the temperature of the given sample but also by its thermal and formation history.^{4,5} Nevertheless, the immediate environment at the molecular level, denoted here as compounds' speciation,⁶ must be crucial for the relevant (photo) reactivity, which is the topic of an ongoing scientific effort,^{7,8} and also constitutes an issue of key importance for atmospheric models.^{4,9} Selected examples of distinct speciation and therefore distinct energy states can consist in solvated separated molecules in ice or (frozen) solutions, molecules on ice surfaces, aggregated molecules in these environments, and crystallized molecules. A major speciation-related question that, to the best of our knowledge, has not been addressed in the literature thus far is how ice temperature affects the crystallinity of aromatic adsorbate layers.

The adsorption of various compounds on (and/or diffusion through) ice was studied in a number of field and laboratory-based experiments utilizing, for example, nitrogen,¹⁰ formaldehyde,^{11,12} acetaldehyde,^{12,13} acetic acid,^{14–20} acetone,^{21–23} acetonitrile,²⁴ dichloromethane,²⁵ HCl,^{26–31} other hydrogen

halides,³² HNO₃,^{33–35} NO₂,³⁶ alkanes,³⁷ alcohols,^{20,38} Xe, Kr, CF₄,³⁹ and other light gases.⁴⁰ The environmental aspects of the adsorption of gases on the ice surface were previously excellently reviewed^{41,42} and remain a subject of active research. However, studies of the adsorption of aromatic compounds on ice are rather limited; for example, a few model aromatic compounds (including benzene and toluene) were deposited on nongrowing ice crystals at 253 K, leaving no impurities after the deposition in/on the ice.⁴³ Similarly, codeposition was performed on growing ice crystals, with only some of the studied compounds detected in the prepared sample.⁴⁴ Benzene was found not to form multilayers on the ice surface.⁴⁵ The saturation surface coverage increased with rising temperature as the thickness of the quasi-liquid layer affects the adsorption. Phenanthrene was adsorbed on natural snow and proved to be deposited by adsorption onto the surface rather than incorporated into the ice matrix.⁴⁶ Later, the thermodynamic parameters for the adsorption on the quasi-liquid layer of ice were found to be similar to those for the water surface.⁴⁷ The adsorption of 1-methylnaphthalene at 238 K allowed monomeric and excimeric emission at low coverages and higher final concentrations, respectively.⁴⁸ The benzene vapor deposited on the ice exhibited different emission properties compared to those of the frozen aqueous solution.⁴⁹

Received: April 27, 2018

Revised: May 3, 2018

Published: May 10, 2018

Few computational simulations were performed for the adsorption of aromatic molecules (benzene, naphthalene, anthracene, and phenanthrene) to the ice surfaces.^{46,48–53} All the research reports agree that the aromatic molecules would preferentially arrange in parallel with the ice surface. Recently, the adsorption of aromatic molecules on the ice surface with gradually increasing coverage was studied by the grand canonical Monte Carlo simulation at 200 K.⁵⁰ At low surface coverages, specific interactions between the ice and the molecules prevail, forming relatively strong OH– π hydrogen bonds with dangling OH bonds of the ice surface. At higher surface coverages, however, the newly arriving aromatic molecules could not bind with the ice surface that strongly; instead, they interacted more with the other adsorbed molecules via lateral interactions. Therefore, if there is enough mobility allowed after the adsorption on the ice surface, the molecules are likely to aggregate and form mixed aqueous aromatic grains.

The speciation of the compounds in the environment influences not only their reactivity but also further interactions. The compounds present exhibit increased roughness as compared to that of the pure ice surface; thus, they provide more adsorption sites^{54,55} or can better function as crystallization nuclei.⁵⁶ Adsorption on ice may also increase the thickness of a disordered interface, such that it becomes markedly more reactive. This situation is thought to occur in polar stratospheric clouds to play a role in springtime ozone depletion.³⁰

Naphthalene is the simplest polycyclic aromatic hydrocarbon and, as such, can be seen as a representative of this family of pollutants important in natural environments.^{57–60} It is known that polycyclic aromatic hydrocarbons are present in the interstellar medium mostly in the gas phase; under certain conditions, they condense on interstellar grains or incorporate within interstellar ices.⁶¹ Furthermore, naphthalene was recognized as a significant factor in the formation of secondary atmospheric aerosols,⁶² and it also constitutes a good fluorescent molecular probe with amply described spectroscopy.^{63–68} Naphthalene was applied to characterize various chemical environments,^{69–71} including frozen aqueous solutions.^{48,52,72–74} Naphthalene belongs to volatile aromatic compounds having a relatively high vapor pressure (11.4 Pa at 298.49 K)⁷⁵ and thus can be easily distributed to the surfaces from the gas phase. It was also shown by the fluorescence emission spectra of naphthalene on a gold substrate that the temperature of deposition has a major impact: vapor deposition below 40 K forms amorphous naphthalene exhibiting excimeric emission only, whereas deposition at 100 K allows both the amorphous and the crystalline modifications.⁷⁶

The purpose of this paper is to investigate, on naphthalene as the model system,⁷⁷ how the temperature of deposition from the gas phase and the thermal history of water ice (I_h) influence molecular speciation. We detail the conditions under which the formation of microscopic crystals is the prevalent output of the vapor deposition. To this end, we have studied the adsorption of naphthalene at two distinct temperatures, namely, 77 and 253 K. These serve as model temperatures for ice surfaces in astrophysical environments such as interstellar clouds or icy moons and are also applied for earth-based ice surfaces, such as a snowpack or tropospheric ice clouds.

■ EXPERIMENTAL PART

The naphthalene (pure) was purchased from the Lachema company. The artificial snow (ice spheres) for the vapor deposition was prepared by spraying distilled or deionized water into liquid nitrogen. The deposition of the naphthalene vapor on the ice spheres' surfaces was performed using a dedicated apparatus (represented in Figure S1); the device comprises a glass finger into which the snow layer can be placed. The nitrogen gas carrying the naphthalene vapor enters this finger through a chamber filled with naphthalene crystals immobilized by cotton wool. The finger, together with the whole vapor deposition apparatus, was precooled by a coolant (liquid nitrogen or ethanol cooled down to 253 K). The nitrogen carrier gas from the cylinder (4.0, SIAD Czech spol. s r.o.) was also precooled by being forced to flow through a silicon hose immersed in the liquid nitrogen. All the depositions were performed at atmospheric pressure and proceeded for the indicated time. After this stage, a part of the naphthalene-deposited ice spheres was removed from the glass finger, homogenized (using a precooled spatula to ensure representative sampling for the luminescence analysis), and placed into a quartz cuvette precooled to 77 K; subsequently, the fluorescence was measured in a cryostat within the indicated range of temperatures. In the deposition at 77 K, the fluorescence measurements started at 77 K, and the temperature gradually increased, following the steps indicated for each experiment. As regards the vapor deposition at 253 K, the first measurement was performed at 253 K, with the temperature subjected to progressive reduction, as also indicated for each particular experiment.

The fluorescence measurements were carried out on an FLS 920 fluorescence spectrometer (Edinburgh Instruments) equipped with a 450 W Xe lamp, a PMT detector, and a double grating monochromator. We used quartz cuvettes in an Optistat DN2 cryostat (Edinburgh Instruments) configured via the front face geometry to collect the light from the face on which the excitation light was incident. The stability tests were performed for up to 5 h, yielding no significant spectral appearance changes. The differential scanning calorimetry (DSC) measurements employed a PerkinElmer DSC 8000 calorimeter, and the X-ray diffractograms were measured on a Siemens D5000 diffractometer in the θ – θ geometry, using Cu $K\alpha_1$ radiation ($\lambda = 1.54 \text{ \AA}$).

■ RESULTS

Naphthalene vapor deposition on the ice spheres was performed at two distinct temperatures, 77 and 253 K, resulting in significantly different naphthalene fluorescence emission spectra.

Vapor Deposition at 77 K. The fluorescence emission spectrum of naphthalene prepared by deposition at 77 K for 30 min is shown in Figure 1. Two distinct spectral features were observed, namely, the emission spectrum of the vibrationally resolved naphthalene monomer spanning the range between 300 and 360 nm and a broad structureless band centered at 395 nm, as is typical of the excimer. The matching of all the examined excitation spectra (shown are those recorded at $\lambda_{em} = 370, 395,$ and 430 nm) with the absorption spectrum (not presented) confirms that both the emission bands originated from the naphthalene and not from an impurity.⁵²

The relative intensity of the 395 nm band decreases with rising temperature (Figures 2, S2–S4), while the emission

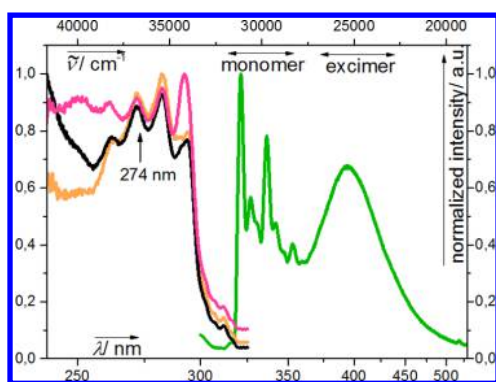


Figure 1. Fluorescence excitation ($\lambda_{\text{em}} = 370$ nm, orange; $\lambda_{\text{em}} = 395$ nm, black; $\lambda_{\text{em}} = 430$ nm, magenta) and emission spectra ($\lambda_{\text{exc}} = 274$ nm, green) of the naphthalene vapor deposited (for 30 min) on the ice spheres at 77 K.

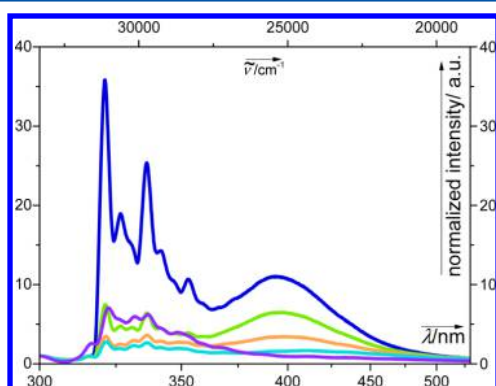


Figure 2. Temperature dependence of the fluorescence emission spectra ($\lambda_{\text{exc}} = 274$ nm) of the naphthalene vapor deposited at 77 K. The measurement temperature: 77 K—blue; 100 K—green; 133 K—orange; 160 K—cyan; and 253 K—violet. All the spectra were normalized to 1 at $\lambda = 300$ nm.

intensity of the monomer decreases for the temperatures of between 77 and 160 K and increases upon further warming at temperatures of 253 K and higher. The estimated relative intensities of the observed emissions are shown in Figure S3. The given results are highly reproducible. The figures visualize the most representative spectra of the 18 repetitive experiments we conducted.

Occasionally (in 4 out of the 18 samples), a vibrational structure at 398, 402, and 431 nm was superimposed on the broad excimer band (Figure S2), which, based on previous experiments,^{72,78} we attribute to the sensitized emission from anthracene impurity. In one of the experiments, the excimeric emission was completely missing and was fully substituted with that of anthracene (Figure S5). In cases where both the anthracene monomer and the naphthalene excimer emissions appeared, we mathematically subtracted the spectra at different temperatures to distinguish more clearly between the monomeric and the excimeric emission signals of the naphthalene (Figure 3).

Vapor Deposition at 253 K. The naphthalene vapor deposition at 253 K was performed for the time durations of between 15 and 60 min. The detected emission spectra always show the vibrationally resolved signals in the region of 300–380 nm and, in contrast to the vapor deposition at 77 K, never display any signs of the broad excimer band (Figure 4). The observed signals resemble those of the monomer emission

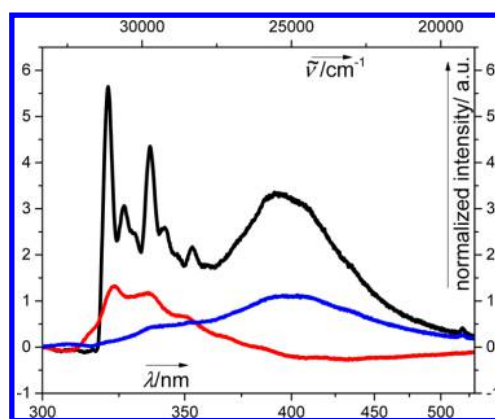


Figure 3. Difference spectra after the subtraction of the anthracene fluorescence at 200 K (black: 77–200 K; blue: 133–200 K; red: 253–200 K). The original spectra and the subtraction procedure are detailed in Figure S2.

(300–380 nm), with extra peaks at 385, 415, and 434 nm caused by anthracene.

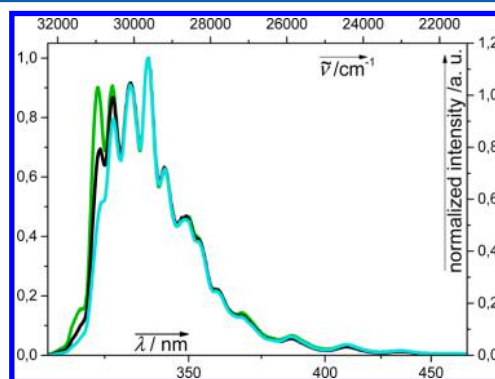


Figure 4. Fluorescence emission spectra ($\lambda_{\text{exc}} = 274$ nm) of the naphthalene vapor deposited at 253 K; the dependence on the deposition time: 15 min—green; 30 min—black; and 60 min—cyan.

We assign the observed emission spectra of the naphthalene vapor deposited at 253 K to the spectra of the naphthalene crystals, based on the following observations and arguments: the difference in the vapor-deposited spectra at 253 K with consecutive time durations lies only in the decreased emission intensity at the blue edge of the emission spectra (around 323 nm) (Figure 4) and can be well-described as the reabsorption of the emitted light within the naphthalene crystals.

The amount of light reabsorption is directly proportional to the crystal thickness.^{79,80} To ascertain the origin of the emission reabsorption, the spectra of crystals of various thicknesses were compared: those of the naphthalene vapor deposited at 253 K; that of the naphthalene thin film (made from the naphthalene solution via evaporation of methanol); that of the powdered naphthalene crystals (pulverized in a mortar); and that of the coarse macroscopic crystals (Figure 5). The relative intensity of the bands at the blue edge (from around 312 to 338 nm) decreases within the spectra in the following order: the naphthalene vapor deposited (253 K), the naphthalene thin film, the powdered naphthalene crystals, and the macroscopic naphthalene crystals. The most pronounced reabsorption occurs in the case of the coarse naphthalene crystals of millimetric thickness. All the above-mentioned spectra are very similar in the wavelength range of 335–500 nm. Therefore, it

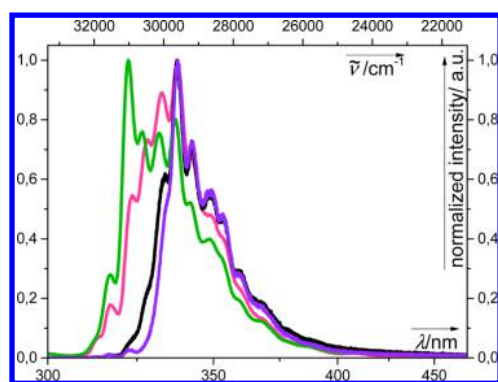


Figure 5. Fluorescence emission spectra ($\lambda_{\text{exc}} = 274 \text{ nm}$) of the naphthalene: the vapor-deposited sample at 253 K (253 K, green); the thin crystalline film (298 K, pink); the powdered naphthalene crystals (253 K, black); and the macroscopic crystals (253 K, purple).

can be concluded that the vapor deposition at this temperature (253 K) most probably causes the crystals' formation.

The ice samples with the naphthalene vapor deposited at both the above temperatures were analyzed by DSC and X-ray spectroscopy.

Differential Scanning Calorimetry. After the vapor deposition, we placed a part of the ice spheres into a sample pan and measured their differential scanning calorimetry at temperatures between 93 K ($-180 \text{ }^\circ\text{C}$) and 363 K ($90 \text{ }^\circ\text{C}$) (Figure 6), with the heating rate of 30 K min^{-1} . For the

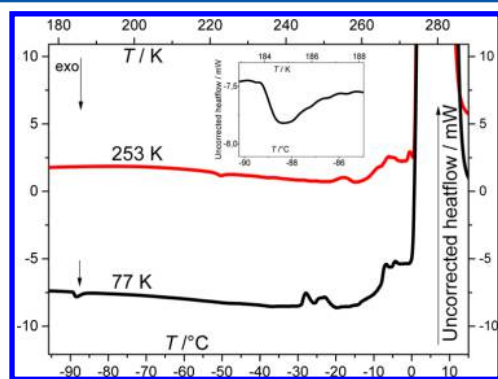


Figure 6. DSC measurements of the naphthalene deposited at 253 K (red) and 77 K (black), both measured between 93 K ($-180 \text{ }^\circ\text{C}$) and 363 K ($90 \text{ }^\circ\text{C}$). The subset depicts the devitrification at 185 K ($-88 \text{ }^\circ\text{C}$) for the naphthalene deposited at 77 K.

naphthalene deposited at 77 K, we assigned the exothermic peak at 185 K ($-88 \text{ }^\circ\text{C}$, marked with an arrow on the black calorigram) to the devitrification of the amorphous naphthalene. The peak is not very sharp, and its asymmetry indicates that the process exhibits slow transformation kinetics. The crystallization heat associated with this peak results from the transformation of the initially amorphous deposit to a polycrystalline one. The endothermic peaks in the temperature range of between 243 K ($-30 \text{ }^\circ\text{C}$) and 273 K ($0 \text{ }^\circ\text{C}$) can be related to the desorption and/or sublimation of the naphthalene crystals from the ice. The massive endotherm at $0 \text{ }^\circ\text{C}$ indicates the melting of the ice itself. For the naphthalene deposited at 253 K, no significant heat change was observed below 253 K ($-30 \text{ }^\circ\text{C}$). The small endotherms above this temperature indicate again the desorption or sublimation of the naphthalene.

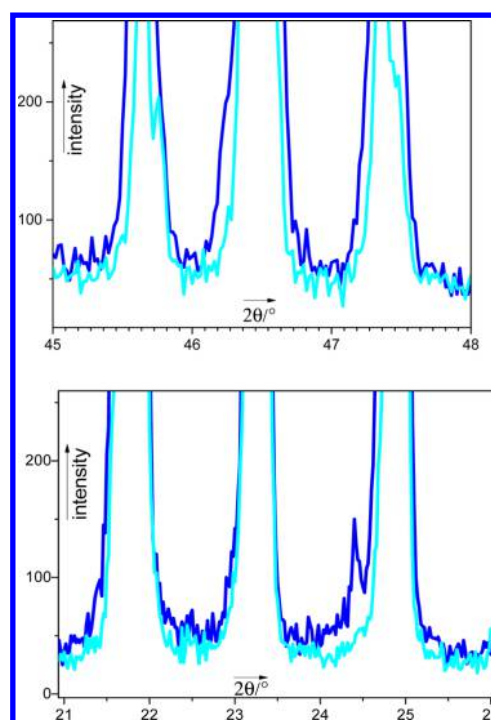


Figure 7. X-ray diffractograms of the naphthalene vapor deposited at 77 K (dark blue) and 253 K (cyan), both measured at 80 K.

X-ray. The X-ray diffractograms are not very sensitive to the surface layer of the naphthalene. All that can be seen in Figure 7 (and Figures S6 and S7) are the Bragg peaks originating from the ice I_h . Almost no difference is discernible between the two samples; however, the Bragg peaks for the samples deposited at 77 K are notably broader than those found after the vapor deposition at 253 K. This observation can be explained in two ways: either by the sintering of the ice crystals at 253 K, forming ice crystals of a slightly smaller size, or, more likely, by the amorphous layer of naphthalene at 77 K. The interaction with the amorphous layer might distort the ice surface, especially if the naphthalene molecules cluster in domains. This effect of a nonuniform surface layer causing the distribution of the lattice constants is minimized after the naphthalene crystallization, that is, the formation of a more uniform ice layer (Figure S7).

DISCUSSION

The fluorescence emission spectra of the naphthalene vapor deposited on the ice spheres at 77 K (Figure 1) show characteristics of the naphthalene amorphous structure, namely, the monomer emission and that of the excimer with the maximum at 395 nm, comparable to those on inert surfaces, such as gold⁷⁶ or glass.⁶⁹ Such an excimeric emission is typical of not only the amorphous arrangement as confirmed by the IR spectra⁸¹ but also nonaqueous concentrated solutions;^{82–85} it differs from the excimeric emission found in silica glasses,⁷⁰ Na–Y zeolites,⁸⁶ or frozen aqueous solutions,^{52,72} which possess emission maxima at lower wavelengths (375 nm) strongly overlapping with the monomer emission (see Figure S8). The 375 nm excimer was assigned to the emission from the “second excimer” formed from the ground-state dimer, based on kinetic analysis.⁷⁰ The observed excimeric emission also contrasts the purely monomeric signal found in the codeposited water–naphthalene ice prepared at 15 K.⁶⁸ We can

infer from these comparisons that the naphthalene deposition rate in our experimental arrangement is faster than that of water from the sublimating ice,⁸⁷ thus facilitating the formation of the naphthalene amorphous glass layer on the ice surface rather than an adlayer mixed with water, in which the excimer formation would not be expected. As the crystalline naphthalene is very difficult to purify from traces of anthracene, its presence was noticed in some of our samples (Figures S2, 4, and S5) and then advantageously employed to gather additional information about the ice impurities. The energy transfer from the naphthalene to the locations of the excimeric naphthalene and to the anthracene constitutes two possibly competing pathways: the first process is temperature-dependent, whereas the second one seems to be temperature-independent. The temperature independence of the energy transfer to the anthracene can be inferred from Figure 3, where the subtraction of the spectra at 200 K—in which case the energy transfer to the anthracene prevailed—shows naphthalene spectra very similar to those with no anthracene emission. Both the cases of observed luminescence provide clear information about the arrangement on the ice surface: the molecules must be aggregated closely enough within the domain where the energy transfer is possible. The excitation spectra (shown only in one case) confirm that in any condition applied herein, the absorption characteristics of the naphthalene do not red-shift compared to the aqueous solution spectra, as also observed for frozen solutions.^{48,49,52} However, the polar organic molecules with functional groups may be markedly more sensitive to the solvatochromic influence of the ice surface⁸⁸ or aggregation.⁸⁹ Importantly, in this context, the unaltered excitation spectra detected at multiple wavelengths (Figure 1) also provide an argument for unbiased evaluation of the relative intensity of the monomeric and excimeric species in the emission spectra at various temperatures.

Figure 2 shows the evolution of the temperature dependence of the fluorescence emission spectra for the ice spheres with the naphthalene deposited at 77 K. The first fact to be noticed, in sharp contrast with the emission observed from the macroscopic crystals (Figure 5), is the absence of self-absorption at the blue edge of the emission spectra. This confirms the conclusions related to the amorphous nature of the layer formed, where the statistical distribution of the molecular orientation can be expected: some molecules exhibit monomeric emission, whereas others display the excimeric form. The emitted light is not absorbed noticeably; we cannot conclude whether this is due to the small thickness of the layer or its porosity and reflective properties. The self-absorption does not appear even with increasing temperature, indicating the formation of very thin crystalline structures. The confirmation of this fact originates also from the close resemblance of these spectra to those of the thin crystals, as detailed in Figure S9. In view of these facts, it is then possible to propose that the absence of self-absorption allows us to compare the relative intensities of the monomer and excimer emission ratio. Upon warming, the fluorescence emission spectra of the naphthalene deposited on the ice spheres at 77 K evolve in the following manner: at temperatures below 100 K, the monomeric emission diminishes at the expense of the excimeric one. With further warming, the excimeric signal decreases to full extinction at around 200 K. Given this temperature range, the monomeric signal gradually increases, as indicated in Figure 2. The relative increase of the excimeric emission below 100 K is most likely due to the thermally activated energy transfer to the excimer;

otherwise, it can be ascribed to the volume decrease often observed during warming vapor deposited amorphous structures.⁹⁰ This dependence was previously observed for amorphous naphthalene on gold surfaces: the approximately equal fluorescence intensities of the monomer and the excimer were observed at 40 K, whereas the excimer fluorescence signal prevailed at 100 K.⁷⁶ At higher temperatures, the emission of the excimer was displaced by that of the crystals, corresponding to the crystallization peak at 185 K (−88 °C) on the DSC thermogram and Nakayama's interpretation of his observations.^{76,81} Temperature-induced changes above 190 K do not allow the excimeric emission anymore, even after recooling down to 77 K, indicating the irreversibility of the crystallization (Figure S10). We were surprised not to observe changes of the emission characteristics only after the sample had crystallized at 185 K (value deduced from the DSC). Rather, the excimers' intensity kept decreasing at temperatures above 100 K at the expense of the monomeric signal. The observation is in full accordance with those of the amorphous naphthalene deposited on gold, as measured by the fluorescence⁷⁶ and Raman spectroscopies,⁸¹ where the first signs of naphthalene crystals appeared at 105 K, although full relaxation was achieved only at 190 K during gradual warming. The similarity of our observation to that made on gold suggests that the ice acts as an inert surface and does not influence the naphthalene on the surface at temperatures below 200 K.

Previously, the formation of an amorphous H₂O/HX (X = Cl[−], Br[−], I[−]) adlayer was observed when hydrogen halide gases had been adsorbed to the ice surface at 200 K.³² Interestingly, their adsorption at 110 K allowed only disproportionation reactions on the ice surface, without any sign of amorphous arrangements. Here, we demonstrate for the first time, to the best of our knowledge, that aromatic compounds at 77 K can assemble on the ice surface to form an amorphous material which is possibly technologically utilizable as such materials exhibit some desirable properties, including low β relaxation dynamics.^{90,91}

The X-ray measurements of the ice with the deposited naphthalene did not reveal any signals of naphthalene crystals. Only the Bragg peaks of the I_h ice for the naphthalene deposited at 77 K were found to be broadened compared to those of the pure ice or the naphthalene deposited at 253 K. The variation in the peaks' half-width suggests that the naphthalene might be clustered in amorphous domains distributed on the ice surface. It is expectable that the naphthalene would preferentially deposit on the morphologically protruding parts of the ice. These locations were observed to be more resistant to sublimation than the concave regions.^{92,93} The signals of the ice in the X-ray diffractograms become narrower after the temperature has been raised as the crystallization of the amorphous layer of the naphthalene allows the underlying ice to relax.

The fluorescence spectroscopy measurements have demonstrated that the naphthalene vapor deposited at 253 K does not show any signal besides that of the naphthalene monomer or anthracene. Even with the shortest examined duration of the naphthalene deposition, no sign of excimer emission was observed (Figures 4, S8, and S11). The successive monomeric and excimeric signals could be expected if a critical concentration of the naphthalene on the surface were needed before the crystal formation occurs. The results coincide with the previous observations of the instant appearance of anthracene signals during the deposition of impure naphthalene

from the vapor phase at similar temperatures and also agree with the suggested interpretation of aggregate formation.^{73,94} Thus, the behavior observed by us is independent of the amount of naphthalene deposited, and, as crystals are invariably detected at 253 K, the surface coverages cannot be defined in such instances. The energy transfer to the anthracene is enhanced by this method of preparation; the luminescence of the original naphthalene crystals exhibits less of the characteristic anthracene emission peaks above 380 nm. The vapor deposition at 253 K apparently rendered the energy transfer more efficient in the new arrangement compared to the original crystals. This fact, as well as the increased self-absorption during the prolonged deposition and the similarity of the emission spectra to those of the crystals (Figure 5), embodies a strong indication of the formation of submicrometric crystals on the ice surface. The conclusion is also in accordance with the observed lack of concentration dependence for the apparent rate of photodegradation.⁷³ The photoreactivity of the naphthalene crystals could be expected to be approximately constant, regardless of their size. Unfortunately, no X-ray signal of the naphthalene crystals was observed (Figure 7), which can be explained by the crystals' size being below roughly hundreds of nanometers, based on neutron scattering arguments.⁹⁵ The crystal formation during the vapor deposition at this temperature can be caused by the high mobility on the disordered ice interface, allowing the molecules to translate and aggregate.^{96,97} This conclusion constitutes a sound experimental proof of recent theoretical Monte Carlo simulations, which predicted strong lateral interactions among the aromatic molecules' vapor deposited on the ice surface at 200 K.⁹⁸ The naphthalene surface mobility also agrees with the observed activity of water toward the reactions at comparable temperatures.⁹⁹ Further, our findings confirm those on ice nanoclusters, where picked-up molecules were found not to aggregate at temperatures approximated to be around 100 K.¹⁰⁰ As the timescale of our experiments reaches hours, we can conclude that the initial molecular arrangement on the ice surface remains undisturbed for at least hundreds of minutes if the temperature is controlled.

The compound transport through the vapor phase can take place over long distances at the macroscopic scale of the earth or the interstellar space but also microscopically inside frozen ice samples. For example, if a sample freezes, the volatile impurities can concentrate in the vicinity of the air bubbles,¹⁰¹ where their high vapor pressure can cause resublimation and deposition in the crystalline state, as snow and ice undergo substantial metamorphism at temperatures around 255 K because of the concentration and temperature gradients and fluxes.¹⁰² Therefore, the change of the compound speciation during the ice metamorphosis must be accounted for and possibly included in relevant environmental models.

CONCLUSIONS

This experimental work brings arguments on the strong influence of sample preparation and temperature upon the molecular speciation on ice surfaces. Naphthalene, as a model for aromatic organic pollutants, was found to form an amorphous phase or submicrometric crystals under conditions of atmospheric vapor deposition at 77 or 253 K, respectively. Both of these speciations are distinct from the frozen naphthalene solutions where ground-state interactions (second excimers) dominate over others.⁵² The results have a strong implication for the understanding of impurities in the environment as they clearly exemplify that the actual sample

temperature is only one of the many factors influencing the compounds' speciation: the sample's thermal history is shown to be markedly more important. If vapor deposition on ice occurs at temperatures below 77 K (e.g., in the extraterrestrial space), an amorphous layer can be expected. At relatively high temperatures of atmospheric relevance, the presence of the submicrometer-sized crystals of the pollutants should be considered when their vapor is deposited on the ice surface. The low atmospheric concentrations can be compensated by long deposition exposures. The speciation was found not to depend on the absolute concentration of the naphthalene deposited on the ice sample. The naphthalene molecules applied in this study are to be considered a model for other compounds, and the behavior of such other compounds should be examined at desired concentrations. At the same time, as the described proclivity toward crystallization after the vapor deposition is so contrasting to the behavior after the freezing of the solution, the option of crystal formation should be generally considered also for other molecules. The demonstrated differences in the compound speciation on the ice surface should be taken into consideration when evaluating (photo)chemical reactivity under particular laboratory and, above all, natural conditions.^{103–106}

ASSOCIATED CONTENT

Supporting Information

The Supporting Information is available free of charge on the ACS Publications website at DOI: 10.1021/acs.jpcc.8b03972.

Schema of the vapor deposition apparatus, fluorescence spectra of naphthalene vapor deposited on the ice and frozen solutions of naphthalene, relative intensities of monomer and excimer parts of the spectra as a function of temperature, comparison of the normalization methods, and X-ray spectra (PDF)

AUTHOR INFORMATION

Corresponding Author

*E-mail: hegerd@chemi.muni.cz.

ORCID

Thomas Loerting: 0000-0001-6694-3843

Dominik Heger: 0000-0002-6881-8699

Notes

The authors declare no competing financial interest.

ACKNOWLEDGMENTS

This research was supported by the RECETOX Research Infrastructure (LM2015051 and CZ.02.1.01/0.0/0.0/16_013/0001761) and Czech Science Foundation (GA15-12386S).

REFERENCES

- (1) Bartels-Rausch, T.; Jacobi, H.-W.; Kahan, T. F.; Thomas, J. L.; Thomson, E. S.; Abbatt, J. P. D.; Ammann, M.; Blackford, J. R.; Bluhm, H.; Boxe, C.; et al. A review of air–ice chemical and physical interactions (AICI): liquids, quasi-liquids, and solids in snow. *Atmos. Chem. Phys.* **2014**, *14*, 1587–1633.
- (2) McNeill, V. F.; Grannas, A. M.; Abbatt, J. P. D.; Ammann, M.; Ariya, P.; Bartels-Rausch, T.; Domine, F.; Donaldson, D. J.; Guzman, M. I.; Heger, D.; et al. Organics in environmental ices: sources, chemistry, and impacts. *Atmos. Chem. Phys.* **2012**, *12*, 9653–9678.
- (3) Gudipati, M. S.; Abou Mrad, N.; Blum, J.; Charnley, S. B.; Chiavassa, T.; Cordiner, M. A.; Mousis, O.; Danger, G.; Duvernay, F.;

Gundlach, B.; et al. Laboratory Studies Towards Understanding Comets. *Space Sci. Rev.* **2015**, *197*, 101–150.

(4) Domine, F.; Bock, J.; Voisin, D.; Donaldson, D. J. Can We Model Snow Photochemistry? Problems with the Current Approaches. *J. Phys. Chem. A* **2013**, *117*, 4733–4749.

(5) Krausko, J.; Runštuk, J.; Neděla, V.; Klán, P.; Heger, D. Observation of a Brine Layer on an Ice Surface with an Environmental Scanning Electron Microscope at Higher Pressures and Temperatures. *Langmuir* **2014**, *30*, 5441–5447.

(6) McNaught, A. D. W. A. Chemical species. <https://goldbook.iupac.org/html/C/CT01038.html> (accessed Jan 5, 2018).

(7) Valsaraj, K. T.; Thibodeaux, L. J. On the Physicochemical Aspects of the Global Fate and Long-Range Atmospheric Transport of Persistent Organic Pollutants. *J. Phys. Chem. Lett.* **2010**, *1*, 1694–1700.

(8) Czech, C.; Hammer, S. M.; Bonn, B.; Schmidt, M. U. Adsorption sites, adsorption enthalpies and potential removal of terpenoids by atmospheric ice. *Atmos. Environ.* **2011**, *45*, 687–693.

(9) Thomas, J. L.; Stutz, J.; Lefer, B.; Huey, L. G.; Toyota, K.; Dibb, J. E.; von Glasow, R. Modeling chemistry in and above snow at Summit, Greenland - Part 1: Model description and results. *Atmos. Chem. Phys.* **2011**, *11*, 4899–4914.

(10) Adamson, A. W.; Dormant, L. M.; Orem, M. Physical Adsorption of Vapors on Ice. I. *J. Colloid Interface Sci.* **1967**, *25*, 206.

(11) Barret, M.; Domine, F.; Houdier, S.; Gallet, J.-C.; Weibring, P.; Walega, J.; Fried, A.; Richter, D. Formaldehyde in the Alaskan Arctic snowpack: Partitioning and physical processes involved in air-snow exchanges. *J. Geophys. Res.: Atmos.* **2011**, *116*, D00R03.

(12) Kuo, M. H.; Moussa, S. G.; McNeill, V. F. Surface Disordering and Film Formation on Ice Induced by Formaldehyde and Acetaldehyde. *J. Phys. Chem. C* **2014**, *118*, 29108–29116.

(13) Darvas, M.; Lasne, J.; Laffon, C.; Parent, P.; Picaud, S.; Jedlovsky, P. Adsorption of Acetaldehyde on Ice As Seen from Computer Simulation and Infrared Spectroscopy Measurements. *Langmuir* **2012**, *28*, 4198–4207.

(14) Bertin, M.; Michaut, X.; Lattelais, M.; Mokrane, H.; Pauzat, F.; Pilme, J.; Minot, C.; Ellinger, Y.; Romanzin, C.; Jeseck, P.; et al. Differential Adsorption of Complex Organic Molecule Isomers on Interstellar Ice Surfaces. In *ECLA: European Conference on Laboratory Astrophysics*; Stehle, C., Joblin, C., Dhendecourt, L., Eds.; EDP Sciences: Les Ulis Cedex A, 2013; Vol. 58, pp 349–352.

(15) Bertin, M.; Romanzin, C.; Michaut, X.; Jeseck, P.; Fillion, J.-H. Adsorption of Organic Isomers on Water Ice Surfaces: A Study of Acetic Acid and Methyl Formate. *J. Phys. Chem. C* **2011**, *115*, 12920–12928.

(16) Burke, D. J.; Puletti, F.; Brown, W. A.; Woods, P. M.; Viti, S.; Slater, B. Glycolaldehyde, methyl formate and acetic acid adsorption and thermal desorption from interstellar ices. *Mon. Not. R. Astron. Soc.* **2015**, *447*, 1444–1451.

(17) Křepelová, A.; Bartels-Rausch, T.; Brown, M. A.; Bluhm, H.; Ammann, M. Adsorption of Acetic Acid on Ice Studied by Ambient-Pressure XPS and Partial-Electron-Yield NEXAFS Spectroscopy at 230–240 K. *J. Phys. Chem. A* **2013**, *117*, 401–409.

(18) Lattelais, M.; Bertin, M.; Mokrane, H.; Romanzin, C.; Michaut, X.; Jeseck, P.; Fillion, J.-H.; Chaabouni, H.; Congiu, E.; Dulieu, F.; et al. Differential adsorption of complex organic molecules isomers at interstellar ice surfaces. *Astron. Astrophys.* **2011**, *532*, A12.

(19) Romanias, M. N.; Zogka, A. G.; Papadimitriou, V. C.; Papagiannakopoulos, P. Uptake Measurements of Acetic Acid on Ice and Nitric Acid-Doped Thin Ice Films over Upper Troposphere/Lower Stratosphere Temperatures. *J. Phys. Chem. A* **2012**, *116*, 2198–2208.

(20) Sokolov, O.; Abbatt, J. P. D. Adsorption to ice of n-alcohols (ethanol to 1-hexanol), acetic acid, and hexanal. *J. Phys. Chem. A* **2002**, *106*, 775–782.

(21) Bartels-Rausch, T.; Wren, S. N.; Schreiber, S.; Riche, F.; Schneebeli, M.; Ammann, M. Diffusion of volatile organics through porous snow: impact of surface adsorption and grain boundaries. *Atmos. Chem. Phys.* **2013**, *13*, 6727–6739.

(22) Symington, A.; Leow, L. M.; Griffiths, P. T.; Cox, R. A. Adsorption and Hydrolysis of Alcohols and Carbonyls on Ice at Temperatures of the Upper Troposphere. *J. Phys. Chem. A* **2012**, *116*, 5990–6002.

(23) Peybernès, N.; Le Calvé, S.; Mirabel, P.; Picaud, S.; Hoang, P. N. M. Experimental and Theoretical Adsorption Study of Ethanol on Ice Surfaces. *J. Phys. Chem. B* **2004**, *108*, 17425–17432.

(24) Bhuin, R. G.; Methikkalam, R. R. J.; Sivaraman, B.; Pradeep, T. Interaction of Acetonitrile with Water-Ice: An Infrared Spectroscopic Study. *J. Phys. Chem. C* **2015**, *119*, 11524–11532.

(25) Bhuin, R. G.; Methikkalam, R. R. J.; Bag, S.; Pradeep, T. Diffusion and Crystallization of Dichloromethane within the Pores of Amorphous Solid Water. *J. Phys. Chem. C* **2016**, *120*, 13474–13484.

(26) Ayotte, P.; Marchand, P.; Daschbach, J. L.; Smith, R. S.; Kay, B. D. HCl Adsorption and Ionization on Amorphous and Crystalline H₂O Films below 50 K. *J. Phys. Chem. A* **2011**, *115*, 6002–6014.

(27) Moreira, P. A. F. P.; de Koning, M. Trapping of Hydrochloric and Hydrofluoric Acid at Vacancies on and underneath the Ice I-h Basal-Plane Surface. *J. Phys. Chem. A* **2013**, *117*, 11066–11071.

(28) Olanrewaju, B. O.; Herring-Captain, J.; Grieves, G. A.; Aleksandrov, A.; Orlando, T. M. Probing the Interaction of Hydrogen Chloride with Low-Temperature Water Ice Surfaces Using Thermal and Electron-Stimulated Desorption. *J. Phys. Chem. A* **2011**, *115*, 5936–5942.

(29) Zimmermann, S.; Kippenberger, M.; Schuster, G.; Crowley, J. N. Adsorption isotherms for hydrogen chloride (HCl) on ice surfaces between 190 and 220 K. *Phys. Chem. Chem. Phys.* **2016**, *18*, 13799–13810.

(30) McNeill, V. F.; Loerting, T.; Geiger, F. M.; Trout, B. L.; Molina, M. J. Hydrogen chloride-induced surface disordering on ice. *Proc. Natl. Acad. Sci. U.S.A.* **2006**, *103*, 9422–9427.

(31) McNeill, V. F.; Geiger, F. M.; Loerting, T.; Trout, B. L.; Molina, L. T.; Molina, M. J. Interaction of Hydrogen Chloride with Ice Surfaces: The Effects of Grain Size, Surface Roughness, and Surface Disorder. *J. Phys. Chem. A* **2007**, *111*, 6274–6284.

(32) Barone, S. B.; Zondlo, M. A.; Tolbert, M. A. Investigation of the heterogeneous reactivity of HCl, HBr, and HI on ice surfaces. *J. Phys. Chem. A* **1999**, *103*, 9717–9730.

(33) Marchand, P.; Marcotte, G.; Ayotte, P. Spectroscopic Study of HNO₃ Dissociation on Ice. *J. Phys. Chem. A* **2012**, *116*, 12112–12122.

(34) Moussa, S. G.; Kuo, M. H.; McNeill, V. F. Nitric acid-induced surface disordering on ice. *Phys. Chem. Chem. Phys.* **2013**, *15*, 10989–10995.

(35) Ullerstam, M.; Thornberry, T.; Abbatt, J. P. D. Uptake of gas-phase nitric acid to ice at low partial pressures: evidence for unsaturated surface coverage. *Faraday Discuss.* **2005**, *130*, 211.

(36) Bang, J.; Lee, D. H.; Kim, S.-K.; Kang, H. Reaction of Nitrogen Dioxide with Ice Surface at Low Temperature (≤ 170 K). *J. Phys. Chem. C* **2015**, *119*, 22016–22024.

(37) Orem, M. W.; Adamson, A. W. Physical Adsorption of Vapor on Ice .2. n-Alkanes. *J. Colloid Interface Sci.* **1969**, *31*, 278.

(38) Newberg, J. T.; Bluhm, H. Adsorption of 2-propanol on ice probed by ambient pressure X-ray photoelectron spectroscopy. *Phys. Chem. Chem. Phys.* **2015**, *17*, 23554–23558.

(39) Gibson, K. D.; Langlois, G. G.; Li, W.; Killelea, D. R.; Sibener, S. J. Molecular interactions with ice: Molecular embedding, adsorption, detection, and release. *J. Chem. Phys.* **2014**, *141*, 18C514.

(40) Durão, J.; Gales, L. Permeation of Light Gases through Hexagonal Ice. *Materials* **2012**, *5*, 1593–1601.

(41) Abbatt, J. P. D. Interactions of atmospheric trace gases with ice surfaces: Adsorption and reaction. *Chem. Rev.* **2003**, *103*, 4783–4800.

(42) Huthwelker, T.; Ammann, M.; Peter, T. The uptake of acidic gases on ice. *Chem. Rev.* **2006**, *106*, 1375–1444.

(43) Fries, E.; Haunold, W.; Jaeschke, W.; Hoog, I.; Mitra, S.; Borrmann, S. Uptake of gaseous aromatic hydrocarbons by non-growing ice crystals. *Atmos. Environ.* **2006**, *40*, 5476–5485.

(44) Fries, E.; Starokozhev, E.; Haunold, W.; Jaeschke, W.; Mitra, S.; Borrmann, S.; Schmidt, M. Laboratory studies on the uptake of

aromatic hydrocarbons by ice crystals during vapor depositional crystal growth. *Atmos. Environ.* **2007**, *41*, 6156–6166.

(45) Abbatt, J. P. D.; Bartels-Rausch, T.; Ullerstam, M.; Ye, T. J. Uptake of acetone, ethanol and benzene to snow and ice: effects of surface area and temperature. *Environ. Res. Lett.* **2008**, *3*, 045008.

(46) Domine, F.; Cincinelli, A.; Bonnaud, E.; Martellini, T.; Picaud, S. Adsorption of phenanthrene on natural snow. *Environ. Sci. Technol.* **2007**, *41*, 6033–6038.

(47) Chen, J.; Ehrenhauser, F.; Liyana-Arachchi, T. P.; Hung, F. R.; Wornat, M. J.; Valsaraj, K. T. Adsorption of Gas-Phase Phenanthrene on Atmospheric Water and Ice Films. *Polycyclic Aromat. Compd.* **2011**, *31*, 201–226.

(48) Heger, D.; Nachtigallová, D.; Surman, F.; Krausko, J.; Magyarová, B.; Brumovský, M.; Rubeš, M.; Gladich, I.; Klán, P. Self-Organization of 1-Methylnaphthalene on the Surface of Artificial Snow Grains: A Combined Experimental-Computational Approach. *J. Phys. Chem. A* **2011**, *115*, 11412–11422.

(49) Kania, R.; Malongwe, J. K. E.; Nachtigallová, D.; Krausko, J.; Gladich, I.; Roeselová, M.; Heger, D.; Klán, P. Spectroscopic Properties of Benzene at the Air–Ice Interface: A Combined Experimental–Computational Approach. *J. Phys. Chem. A* **2014**, *118*, 7535–7547.

(50) Mészár, Z. E.; Hantal, G.; Picaud, S.; Jedlovský, P. Adsorption of Aromatic Hydrocarbon Molecules at the Surface of Ice, As Seen by Grand Canonical Monte Carlo Simulation. *J. Phys. Chem. C* **2013**, *117*, 6719–6729.

(51) Liyana-Arachchi, T. P.; Valsaraj, K. T.; Hung, F. R. Adsorption of Naphthalene and Ozone on Atmospheric Air/Ice Interfaces Coated with Surfactants: A Molecular Simulation Study. *J. Phys. Chem. A* **2012**, *116*, 2519–2528.

(52) Krausko, J.; Malongwe, J. K. E.; Bičanová, G.; Klán, P.; Nachtigallová, D.; Heger, D. Spectroscopic Properties of Naphthalene on the Surface of Ice Grains Revisited: A Combined Experimental–Computational Approach. *J. Phys. Chem. A* **2015**, *119*, 8565–8578.

(53) Ardura, D.; Kahan, T. F.; Donaldson, D. J. Self-Association of Naphthalene at the Air–Ice Interface. *J. Phys. Chem. A* **2009**, *113*, 7353–7359.

(54) Romanias, M. N.; Papadimitriou, V. C.; Papagiannakopoulos, P. The Interaction of Propionic and Butyric Acids with Ice and HNO₃-Doped Ice Surfaces at 195–212 K. *J. Phys. Chem. A* **2014**, *118*, 11380–11387.

(55) Hudson, P. K.; Zondlo, M. A.; Tolbert, M. A. The Interaction of Methanol, Acetone, and Acetaldehyde with Ice and Nitric Acid-Doped Ice: Implications for Cirrus Clouds. *J. Phys. Chem. A* **2002**, *106*, 2882–2888.

(56) Murray, B. J.; O’Sullivan, D.; Atkinson, J. D.; Webb, M. E. Ice nucleation by particles immersed in supercooled cloud droplets. *Chem. Soc. Rev.* **2012**, *41*, 6519.

(57) d’Hendecourt, L.; Ehrenfreund, P. Spectroscopic properties of polycyclic aromatic hydrocarbons (PAHs) and astrophysical implications. *Adv. Space Res.* **1997**, *19*, 1023–1032.

(58) Parker, D. S. N.; Zhang, F.; Kim, Y. S.; Kaiser, R. I.; Landera, A.; Kislov, V. V.; Mebel, A. M.; Tielens, A. G. G. M. Low temperature formation of naphthalene and its role in the synthesis of PAHs (Polycyclic Aromatic Hydrocarbons) in the interstellar medium. *Proc. Natl. Acad. Sci. U.S.A.* **2012**, *109*, 53–58.

(59) Rhee, Y. M.; Lee, T. J.; Gudipati, M. S.; Allamandola, L. J.; Head-Gordon, M. Charged polycyclic aromatic hydrocarbon clusters and the galactic extended red emission. *Proc. Natl. Acad. Sci. U.S.A.* **2007**, *104*, 5274–5278.

(60) Ricks, A. M.; Doublerly, G. E.; Duncan, M. A. The Infrared Spectrum of Protonated Naphthalene and its Relevance for the Unidentified Infrared Bands. *Astrophys. J.* **2009**, *702*, 301–306.

(61) Bouwman, J.; Cuppen, H. M.; Steglich, M.; Allamandola, L. J.; Linnartz, H. Photochemistry of polycyclic aromatic hydrocarbons in cosmic water ice II. Near UV/VIS spectroscopy and ionization rates. *Astron. Astrophys.* **2011**, *529*, A46.

(62) Kautzman, K. E.; Surratt, J. D.; Chan, M. N.; Chan, A. W. H.; Hersey, S. P.; Chhabra, P. S.; Dalleska, N. F.; Wennberg, P. O.; Flagan,

R. C.; Seinfeld, J. H. Chemical Composition of Gas- and Aerosol-Phase Products from the Photooxidation of Naphthalene. *J. Phys. Chem. A* **2010**, *114*, 913–934.

(63) Cardinal, J. R.; Mukerjee, P. Solvent Effects on Ultraviolet-Spectra of Benzene-Derivatives and Naphthalene - Identification of Polarity Sensitive Spectral Characteristics. *J. Phys. Chem.* **1978**, *82*, 1614–1620.

(64) George, G. A.; Morris, G. C. The Intensity of Absorption of Naphthalene from 30 000 cm⁻¹ to 53 000 cm⁻¹. *J. Mol. Spectrosc.* **1968**, *26*, 67–71.

(65) Grabner, G.; Rechthaler, K.; Mayer, B.; Köhler, G.; Rotkiewicz, K. Solvent influences on the photophysics of naphthalene: Fluorescence and triplet state properties in aqueous solutions and in cyclodextrin complexes. *J. Phys. Chem. A* **2000**, *104*, 1365–1376.

(66) Passerini, R.; Ross, I. G. Temperature Dependence of the Ultraviolet Absorption Spectrum of Naphthalene in Solution. *J. Chem. Phys.* **1954**, *22*, 1012–1016.

(67) Bree, A.; Thirunamachandran, T. The Crystal Spectrum of Naphthalene in the Region 3200-Å to 2200-Å. *Mol. Phys.* **1962**, *5*, 397–405.

(68) Gudipati, M. S. Matrix-isolation in cryogenic water-ices: Facile generation, storage, and optical spectroscopy of aromatic radical cations. *J. Phys. Chem. A* **2004**, *108*, 4412–4419.

(69) Uchida, K.; Tanaka, M.; Tomura, M. Excimer Emission of Crystalline Naphthalene. *J. Lumin.* **1979**, *20*, 409–414.

(70) Yamanaka, T.; Takahashi, Y.; Uchida, K. Time-resolved fluorescence spectra of naphthalene doped in amorphous silica glasses. *Chem. Phys. Lett.* **1990**, *172*, 405–408.

(71) Forker, R.; Peucker, J.; Meissner, M.; Sojka, F.; Ueba, T.; Yamada, T.; Kato, H. S.; Munakata, T.; Fritz, T. The Complex Polymorphism and Thermodynamic Behavior of a Seemingly Simple System: Naphthalene on Cu(111). *Langmuir* **2014**, *30*, 14163–14170.

(72) Krausko, J.; Ondrušková, G.; Heger, D. Comment on “Photolysis of Polycyclic Aromatic Hydrocarbons on Water and Ice Surfaces” and on “Nonchromophoric Organic Matter Suppresses Polycyclic Aromatic Hydrocarbon Photolysis in Ice and at Ice Surfaces”. *J. Phys. Chem. A* **2015**, *119*, 10761–10763.

(73) Kahan, T. F.; Donaldson, D. J. Photolysis of polycyclic aromatic hydrocarbons on water and ice surfaces. *J. Phys. Chem. A* **2007**, *111*, 1277–1285.

(74) Malley, P. P. A.; Kahan, T. F. Nonchromophoric Organic Matter Suppresses Polycyclic Aromatic Hydrocarbon Photolysis in Ice and at Ice Surfaces. *J. Phys. Chem. A* **2014**, *118*, 1638–1643.

(75) Růžička, K.; Fulem, M.; Růžička, V. Recommended vapor pressure of solid naphthalene. *J. Chem. Eng. Data* **2005**, *50*, 1956–1970.

(76) Nakayama, H.; Hosokawa, T.; Ishii, K. Fluorescence spectra and energy transfer in amorphous naphthalene. *Chem. Phys. Lett.* **1998**, *289*, 275–280.

(77) Burkholder, J. B.; Abbatt, J. P. D.; Barnes, I.; Roberts, J. M.; Melamed, M. L.; Ammann, M.; Bertram, A. K.; Cappa, C. D.; Carlton, A. G.; Carpenter, L. J.; et al. The Essential Role for Laboratory Studies in Atmospheric Chemistry. *Environ. Sci. Technol.* **2017**, *51*, 2519–2528.

(78) Auweter, H.; Braun, A.; Mayer, U.; Schmid, D. Dynamics of Energy-Transfer by Singlet Excitons in Naphthalene Crystals as Studied by Time-Resolved Spectroscopy. *Z. Naturforsch., A: Phys. Sci.* **1979**, *34*, 761–771.

(79) Uchida, K. Reabsorption Effect and Fluorescence Decay Times in Naphthalene Crystals. *Mem. Fukui Inst. Technol.* **1984**, *14*, 121–125. <https://ci.nii.ac.jp/naid/110001194725/en/>.

(80) Ahn, T.-S.; Müller, A. M.; Al-Kaysi, R. O.; Spano, F. C.; Norton, J. E.; Beljonne, D.; Brédas, J.-L.; Bardeen, C. J. Experimental and theoretical study of temperature dependent exciton delocalization and relaxation in anthracene thin films. *J. Chem. Phys.* **2008**, *128*, 054505.

(81) Ishii, K.; Nakayama, H.; Kawahara, M.; Koyama, K.; Ando, K.; Yokoyama, J. Raman-Spectra and Relaxation in Amorphous Naphthalene. *Chem. Phys.* **1995**, *199*, 245–251.

(82) Förster, T. Excimers. *Angew. Chem., Int. Ed.* **1969**, *8*, 333–343.

- (83) Birks, J. B. Excimers. *Rep. Prog. Phys.* **1975**, *38*, 903–974.
- (84) Birks, J. B.; Wright, G. T. Fluorescence Spectra of Organic Crystals. *Proc. R. Soc. London, Ser. B* **1954**, *67*, 657–663.
- (85) Aladekomo, J. B.; Birks, J. B. Excimer Fluorescence .7. Spectral Studies of Naphthalene and its Derivatives. *Proc. R. Soc. London, Ser. A* **1965**, *284*, 551.
- (86) Hashimoto, S.; Hagiri, M.; Matsubara, N.; Tobita, S. Photophysical studies of neutral aromatic species confined in zeolite L: Comparison with cationic dyes. *Phys. Chem. Chem. Phys.* **2001**, *3*, 5043–5051.
- (87) Murphy, D. M.; Koop, T. Review of the vapour pressures of ice and supercooled water for atmospheric applications. *Q. J. R. Meteorol. Soc.* **2005**, *131*, 1539–1565.
- (88) Heger, D.; Klán, P. Interactions of organic molecules at grain boundaries in ice: A solvatochromic analysis. *J. Photochem. Photobiol., A* **2007**, *187*, 275–284.
- (89) Heger, D.; Jirkovský, J.; Klán, P. Aggregation of methylene blue in frozen aqueous solutions studied by absorption spectroscopy. *J. Phys. Chem. A* **2005**, *109*, 6702–6709.
- (90) Ishii, K.; Nakayama, H. Structural relaxation of vapor-deposited molecular glasses and supercooled liquids. *Phys. Chem. Chem. Phys.* **2014**, *16*, 12073.
- (91) Yu, H. B.; Tylinski, M.; Guiseppi-Elie, A.; Ediger, M. D.; Richert, R. Suppression of β Relaxation in Vapor-Deposited Ultrastable Glasses. *Phys. Rev. Lett.* **2015**, *115*, 185501.
- (92) Chen, X.; Shu, J.; Chen, Q. Abnormal gas-liquid-solid phase transition behaviour of water observed with in situ environmental SEM. *Sci. Rep.* **2017**, *7*, 46680.
- (93) Yang, X.; Neděla, V.; Runštuk, J.; Ondrušková, G.; Krausko, J.; Vetráková, L.; Heger, D. Evaporating brine from frost flowers with electron microscopy and implications for atmospheric chemistry and sea-salt aerosol formation. *Atmos. Chem. Phys.* **2017**, *17*, 6291–6303.
- (94) Donaldson, D. J.; Kahan, T. F. Reply to “Comment on ‘Photolysis of Polycyclic Aromatic Hydrocarbons on Water and Ice Surfaces’ and on ‘Nonchromophoric Organic Matter Suppresses Polycyclic Aromatic Hydrocarbon Photolysis in Ice and at Ice Surfaces’”. *J. Phys. Chem. A* **2015**, *119*, 10764–10765.
- (95) Finney, J. L.; Hallbrucker, A.; Kohl, I.; Soper, A. K.; Bowron, D. T. Structures of High and Low Density Amorphous Ice by Neutron Diffraction. *Phys. Rev. Lett.* **2002**, *88*, 225503.
- (96) Grecea, M. L.; Backus, E. H. G.; Fraser, H. J.; Pradeep, T.; Kleyn, A. W.; Bonn, M. Mobility of haloforms on ice surfaces. *Chem. Phys. Lett.* **2004**, *385*, 244–248.
- (97) Park, S.-C.; Moon, E.-S.; Kang, H. Some fundamental properties and reactions of ice surfaces at low temperatures. *Phys. Chem. Chem. Phys.* **2010**, *12*, 12000–12011.
- (98) Mészár, Z. E.; Hantal, G.; Picaud, S.; Jedlovský, P. Adsorption of Aromatic Hydrocarbon Molecules at the Surface of Ice, As Seen by Grand Canonical Monte Carlo Simulation. *J. Phys. Chem. C* **2013**, *117*, 6719–6729.
- (99) Guzmán, M. I.; Hildebrandt, L.; Colussi, A. J.; Hoffmann, M. R. Cooperative hydration of pyruvic acid in ice. *J. Am. Chem. Soc.* **2006**, *128*, 10621–10624.
- (100) Pysanenko, A.; Habartová, A.; Svrčková, P.; Lengyel, J.; Poterya, V.; Roeselová, M.; Fedor, J.; Fárnik, M. Lack of Aggregation of Molecules on Ice Nanoparticles. *J. Phys. Chem. A* **2015**, *119*, 8991–8999.
- (101) Hullar, T.; Anastasio, C. Direct visualization of solute locations in laboratory ice samples. *Cryosphere* **2016**, *10*, 2057–2068.
- (102) Ebner, P. P.; Schneebeli, M.; Steinfeld, A. Metamorphism during temperature gradient with undersaturated advective airflow in a snow sample. *Cryosphere* **2016**, *10*, 791–797.
- (103) Kahan, T. F.; Donaldson, D. J. Benzene Photolysis on Ice: Implications for the Fate of Organic Contaminants in the Winter. *Environ. Sci. Technol.* **2010**, *44*, 3819–3824.
- (104) Ram, K.; Anastasio, C. Photochemistry of phenanthrene, pyrene, and fluoranthene in ice and snow. *Atmos. Environ.* **2009**, *43*, 2252–2259.
- (105) Grannas, A. M.; Bausch, A. R.; Mahanna, K. M. Enhanced aqueous photochemical reaction rates after freezing. *J. Phys. Chem. A* **2007**, *111*, 11043–11049.
- (106) McFall, A. S.; Anastasio, C. Photon flux dependence on solute environment in water ices. *Environ. Chem.* **2016**, *13*, 682.